Frascati Physics Series Vol. XXXVI (2004), pp.
DAΦNE 2004: Physics at meson factories – Frascati, June 7-11 , 2004
Selected Contribution in Plenary Session

RARE HADRONIC B DECAYS

Lluïsa-Maria Mir
Lawrence Berkeley National Laboratory

ABSTRACT

The general methodology to search for rare hadronic B decays, including some examples from the *BABAR* experiment, is presented.

1 Introduction

The Standard Model (SM) has proven to be very healthy so far: the agreement between the theoretical predictions and the experimental results is really good. As a consequence, to find experimental deviations from the SM, we have to study processes that are expected to have small rates, like Cabibbo-Kobayashi-Maskawa (CKM) suppressed decays, or decays dominated by penguin loops. Rare hadronic B decays are well suited for this search because they have, in general, suppressed tree contributions and significant penguins. On the other hand, although rare, these decays are very abundant, and in the past few years there have been many measurements of their branching ratios (BR), asymmetries, etc. In this note, I will describe the general tools used to perform this type of searches, and I will present three particular examples, especially interesting in the way to further test the SM and search for new physics.

2 Analysis method

For fully reconstructed events, the precise knowledge of the beam energy allows the energy and the mass of the reconstructed B to be constrained. The identification of signal events is based on two kinematic variables: the beam–energy substituted mass ($m_{\mathrm{ES}} = \sqrt{(s/2 + \mathbf{p}_i \cdot \mathbf{p}_{\mathrm{B}})^2/E_i^2 - \mathbf{p}_{\mathrm{B}}^2}$) (where the initial four–momentum $(E_i, \mathbf{p_i})$ and the B momentum $\mathbf{p_B}$ are defined in the laboratory frame), and the difference between the reconstructed B energy in the center–of–mass frame and its known value ($\Delta E = E_{\mathrm{B}}^{\mathrm{CM}} - \sqrt{s}/2$).

If the reconstruction was perfect, the difference between the beam and the B energies would be zero, and the reconstructed mass would be the B mass. Even with reconstruction uncertainties, these two variables provide good discrimination against the main background, which comes from continuum production. In B factories the B's are produced almost at rest, and consequently the topology of the events is spherical, whereas continuum events have a two–jet structure. Other typical discriminant variables are the masses of the intermediate resonances, the decay angles, and the decay time difference of the two B's. Some of these distributions are shown in fig.1.

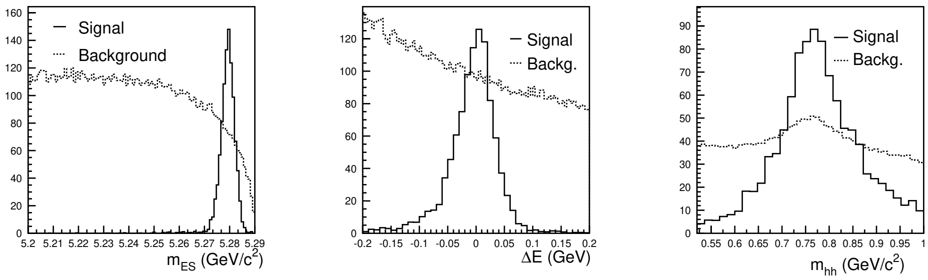

Figure 1: *From left to right: beam–energy substituted mass, energy difference, and resonance mass, for signal (solid) and continuum background (dashed).*

To measure BR's, these distributions are used to build probability density functions, and a likelihood fit is performed to determine signal yields. Difference of decay times and tagging information is included in time–dependent measurements.

3 Examples

3.1 Decays to pairs of isoscalars

We measure the BR's of all (η, η', $\omega\,\phi$) (η, η', $\omega\,\phi$) combinations except $\omega\omega$ and $\omega\phi$. The measured values for a sample of 82M $\mathrm{B\overline{B}}$ events are summarized in tab.1 [1].

Table 1: *BR's of B decays to two isoscalars.*

Mode	S(σ)	$\mathcal{B}(10^{-6})$	UL (10^{-6})	UL (10^{-6}) (CLEO)
$\eta\eta$	0.0	$-0.9^{+1.6}_{-1.4} \pm 0.7$	2.8	18
$\eta\eta'$	0.3	$0.6^{+2.1}_{-1.7} \pm 1.1$	4.6	27
$\eta'\eta'$	0.4	$1.7^{+4.8}_{-3.7} \pm 0.6$	10	47
$\eta\omega$	4.3	$4.0^{+1.3}_{-1.2} \pm 0.4$	6.2	12
$\eta'\omega$	0.0	$-0.2^{+1.3}_{-0.9} \pm 0.4$	2.8	60
$\eta\phi$	0.0	$-1.4^{+0.7}_{-0.4} \pm 0.2$	1.0	9
$\eta'\phi$	0.8	$1.5^{+1.8}_{-1.5} \pm 0.4$	4.5	31
$\phi\phi$	0.3	$0.3^{+0.7}_{-0.4} \pm 0.1$	1.5	12

The upper limits on the BR's have been tightened considerably, and this translates into an improvement of a factor of 2 in the Grossman-Ligeti-Nir-Quinn bound [2] on the difference of the S coefficient of the time–dependent asymmetry measured in $\mathrm{B} \to \mathrm{J}/\psi \mathrm{K^0_S}$ and $\mathrm{B} \to \eta' \mathrm{K^0_S}$ decays.

3.2 BR's and CP asymmetries in $\mathrm{B^0} \to \mathrm{K^+K^-K^0_S}$ and $\mathrm{B^+} \to \mathrm{K^+K^0_SK^0_S}$

B decays to three kaons are interesting because there is a 2.7 σ discrepancy between the *BABAR* and Belle results in the measured S coefficient of the time–dependent asymmetry in the $\mathrm{B} \to \phi \mathrm{K^0_S}$ decay. The measurement of the B decay to three kaons, integrated over all the phase–space, has the advantage over $\mathrm{B} \to \phi \mathrm{K^0_S}$ of a better statistical precision due to the larger data sample. On the other hand, the CP–content of the final states is unknown and has to be measured. This is done using the isospin symmetry relation:

$$f_{\mathrm{even}} = \frac{N_{CP}}{N} = \frac{\Gamma(\mathrm{B}^+ \to \mathrm{K}^+\mathrm{K}^0_\mathrm{S}\mathrm{K}^0_\mathrm{S})}{\Gamma(\mathrm{B}^0 \to \mathrm{K}^+\mathrm{K}^-\mathrm{K}^0)} \tag{1}$$

Figure 2 shows the Δt distributions for B^0 and $\overline{\mathrm{B}^0}$ decays and the results of the fits for a sample of 124M $\mathrm{B}\overline{\mathrm{B}}$ events are listed in tab.2 [3]. Finally, tab.3 shows a comparison of the *BABAR* and Belle results on CP–asymmetries for $\phi\mathrm{K}^0$ and $\mathrm{KKK}^0_\mathrm{S}$. The agreement in the three–kaon channel is good.

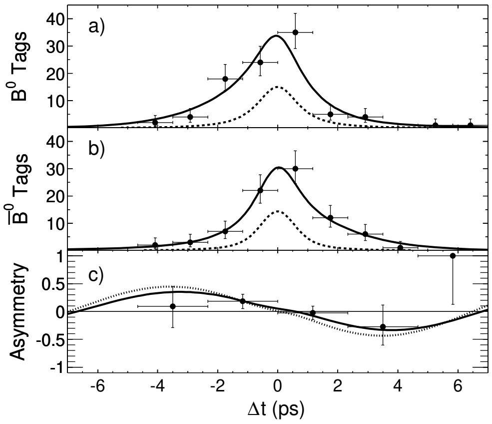

Figure 2: *Plots a) and b) show the Δt distributions of* B^0*– and* $\overline{\mathrm{B}^0}$*–tagged* $\mathrm{K}^+\mathrm{K}^-\mathrm{K}^0_\mathrm{S}$ *events. Solid lines correspond to all events and dashed lines to background. Plot c) shows the raw asymmetry, where the solid line is obtained from the fit and the dotted line corresponds to the SM expectation.*

3.3 Angular analysis in $\phi\mathrm{K}^*$ decays

The angular distribution of the decay of a B meson to a vector pair is unknown a priori, but can be parameterized as a function of the decay angles and the helicity amplitudes as follows:

Table 2: *Summary of BR's ($\mathcal{B}$), time–dependent (S,C) and direct CP–asymmetry ($\mathcal{A}_{\rm CP}$) results;* $\rm f_{even}$ *is the fraction of CP–even final states.*

	$(\rm K^+K^-K^0)^{CP}$	$(\rm K^+K^-K^0)^{all}$	$\rm K^+K^0_SK^0_S$
$\mathcal{B}\,(10^{-6})$	$20.2 \pm 1.9 \pm 1.4$	$23.8 \pm 2.0 \pm 1.6$	$10.7 \pm 1.2 \pm 1.0$
$\rm f_{even}$	$0.98 \pm 0.15 \pm 0.04$	$0.83 \pm 0.12 \pm 0.03$	–
S	$-0.56 \pm 0.25 \pm 0.04$	–	-0.16 ± 0.35
C	$-0.10 \pm 0.19 \pm 0.10$	–	-0.08 ± 0.22
$\mathcal{A}_{\rm CP}$	–	–	$-0.04 \pm 0.11 \pm 0.02$

Table 3: *Comparison of BABAR and Belle measurements on time–dependent asymmetries for three kaon decays.*

$-\eta_{\rm f} \times \rm S_f$	$\phi \rm K^0$	$\rm KKK^0_S$
BABAR	$0.47 \pm 0.34^{+0.08}_{-0.06}$	$0.56 \pm 0.25 \pm 0.04^{+0.17}_{-0.00}$
Belle	$-0.96 \pm 0.50^{+0.09}_{-0.11}$	$0.51 \pm 0.26 \pm 0.05^{+0.18}_{-0.00}$
Average	0.02 ± 0.29 (0.28 stat only)	$0.54 \pm 0.18^{+0.17}_{-0.00}$ (0.18 stat only)

$$
\begin{aligned}
\frac{1}{\Gamma}\frac{d^3\Gamma}{d\cos\theta_1 d\cos\theta_2 d\Phi} = \frac{9}{8\pi}\frac{1}{|A_0|^2+|A_{+1}|^2+|A_{-1}|^2} \times \\
\Big\{ \frac{1}{4}\sin^2\theta_1\sin^2\theta_2\left(|A_{+1}|^2+|A_{-1}|^2\right)+\cos^2\theta_1\cos^2\theta_2|A_0|^2+ \\
\frac{1}{2}\sin^2\theta_1\sin^2\theta_2\left[\cos 2\Phi Re(A_{+1}A^*_{-1})-\sin 2\Phi Im(A_{+1}A^*_{-1})\right]- \\
\frac{1}{4}\sin 2\theta_1 \sin 2\theta_2\left[\cos\Phi Re\left(A_{+1}A^*_0+A_{-1}A^*_0\right)-\sin\Phi Im\left(A_{+1}A^*_0-A_{-1}A^*_0\right)\right]\Big\} \qquad (2)
\end{aligned}
$$

The quantities that are obtained from the fit are the total number of events ($n_{\rm sig}$), the fractions of longitudinal ($f_{\rm L} = \frac{|A_0|^2}{\sum_m |A_m|^2}$), and transverse ($f_\perp = \frac{|A_\perp|^2}{\sum_m |A_m|^2}$) polarization, and the phases ($\phi_\parallel = arg(A_\parallel) - arg(A_0)$ and $\phi_\perp = arg(A_\perp) - arg(A_0)$). If differences between the $\rm B^0$ and $\rm \overline{B^0}$ decay amplitudes are allowed, we can define the following CP–violating asymmetries or differences: $\mathcal{A}_{\rm CP} = \frac{\rm n^+_{sig} - n^-_{sig}}{\rm n^+_{sig}+n^-_{sig}}$ (direct CP-asymmetry), $\mathcal{A}^0_{\rm CP} = \frac{\rm f^+_L - f^-_L}{\rm f^+_L + f^-_L}$ (longitudinal asymmetry), $\mathcal{A}^\perp_{\rm CP} = \frac{\rm f^+_\perp - f^-_\perp}{\rm f^+_\perp + f^-_\perp}$ (transverse asymmetry), $\Delta\phi_\parallel = \frac{1}{2}(\phi^+_\parallel - \phi^-_\parallel)$

(CP-even) and $\Delta\phi_\perp = \frac{1}{2}(\phi_\perp^+ - \phi_\perp^-)$ (CP-odd).

The results of the fit for a sample of 124M $B\overline{B}$ events are summarized in tab.4 [4]. The surprising result is the fitted value of the longitudinal–polarization fraction, which is expected to be approximately 1 in the SM. We can visualize these results in the two–dimensional contours shown in fig.3.

Table 4: $B \to \phi K^{*0}$ *fit results.*

$n_{\rm sig}$	f_L	$f_\perp$	$\phi_\parallel$
$129 \pm 14 \pm 9$	$0.52 \pm 0.07 \pm 0.02$	$0.27 \pm 0.07 \pm 0.02$	$2.63^{+0.24}_{-0.23} \pm 0.04$
$\phi_\perp$	$\mathcal{A}_{\rm CP}$	$\mathcal{A}^0_{\rm CP}$	$\mathcal{A}^\perp_{\rm CP}$
$2.71^{+0.22}_{-0.24} \pm 0.03$	$-0.12 \pm 0.10 \pm 0.03$	$-0.02 \pm 0.12 \pm 0.01$	$-0.10^{+0.25}_{-0.27} \pm 0.04$
$\Delta\phi_\parallel$		$\Delta\phi_\perp$	
$0.38^{+0.23}_{-0.24} \pm 0.04$		$0.30^{+0.24}_{-0.22} \pm 0.03$	

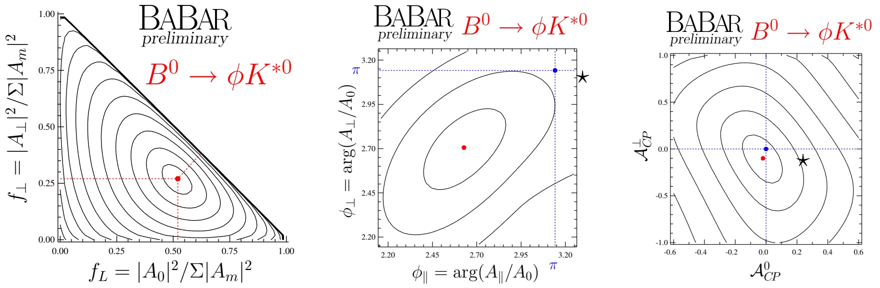

Figure 3: *From left to right: two–dimensional contour of longitudinal versus transverse polarization fraction, CP–odd versus CP–even phase, and transverse versus longitudinal asymmetry. The points correspond to the measured values and the stars to the SM expectations.*

References

1. B.Aubert *et al.* [*BABAR*] Sub. to Phys. Rev. Lett. (hep-ex/0403046).

2. Y.Grossman *et al.*, Phys. Rev. D **68**, 015004 (2003).

3. B.Aubert *et al.* [*BABAR*] Sub. to Phys. Rev. Lett. (hep-ex/0406005).

4. B.Aubert *et al.* [*BABAR*] Sub. to Phys. Rev. Lett. (hep-ex/0408017).